Limb-Girdle Muscular Dystrophy Type 2A Can Result from Accelerated Autoproteolytic Inactivation of Calpain 3[†]

Christopher P. Garnham,[‡] Rachel A. Hanna,[‡] Jordan S. Chou,[‡] Kristin E. Low,[‡] Keith Gourlay,[‡] Robert L. Campbell,[‡] Jacques S. Beckmann,[§] and Peter L. Davies*[,‡]

Department of Biochemistry, Queen's University, Kingston, Ontario, Canada K7L 3N6, and Service and Department of Medical Genetics, Centre Hospitalier Universitaire Vaudois, CHUV, and Faculty of Biology and Medicine, University of Lausanne, Lausanne, Switzerland

Received January 27, 2009; Revised Manuscript Received February 17, 2009

ABSTRACT: Loss-of-function mutations in calpain 3 have been shown to cause limb-girdle muscular dystrophy type 2A (LGMD2A), an autosomal recessive disorder that results in gradual wasting of the muscles of the hip and shoulder areas. Due to the inherent instability of calpain 3, recombinant expression of the full-length enzyme has not been possible, making *in vitro* analysis of specific LGMD2A-causing mutations difficult. However, because calpain 3 is highly similar in amino acid sequence to calpain 2, the recently solved crystal structure of full-length, Ca^{2+}-bound, calpastatin-inhibited rat calpain 2 has allowed us to model calpain 3 as a Ca^{2+}-bound homodimer. The model revealed three distinct areas of the enzyme that undergo a large conformational change upon Ca^{2+} binding. Located in these areas are several residues that undergo mutation to cause LGMD2A. We investigated the *in vitro* effects of six of these mutations by making the corresponding mutations in rat calpain 2. All six mutations examined in this study resulted in a decrease in enzyme activity. All but one of the mutations caused an increased rate of autoproteolytic degradation of the enzyme as witnessed by SDS−PAGE, indicating the decrease in enzyme activity is caused, at least in part, by an increase in the rate of autoproteolytic degradation. The putative *in vivo* effects of these mutations on calpain 3 activity are discussed with respect to their ability to cause LGMD2A.

The first member of the calpain family of Ca^{2+}-activated neutral cysteine proteases was identified over 40 years ago in the soluble fraction of rat brain extracts (*1*). Since then, homologues of the enzyme have been found in diverse organisms, often with multiple isoforms present within individual species (*2*) or even within a single gene. To date, 14 calpain genes have been found in humans, 4 in *Drosophila melanogaster* and 12 in *Caenorhabditis elegans*. With their ability to cleave a wide variety of target proteins in a limited and specific manner in response to Ca^{2+} signaling, the calpains play a key role in the regulation of many cellular processes including cell motility (*3*), signal transduction (*4*), cell cycle progression (*5*), apoptosis (*6*), and gene expression (*7*). Not surprisingly, several pathologies have been linked to the misregulation of other calpains, and these include type 2 diabetes (*8, 9*), limb-girdle muscular dystrophy (*10*), Alzheimer's disease (*11, 12*), cataract formation (*13, 14*), and multiple sclerosis (*15*), among others.

The most extensively studied members of the calpain family are calpains 1 and 2, also known as μ- and m-calpain, respectively. They are ubiquitously expressed in all tissues, and each forms a heterodimer with the inappropriately named calpain 4, which is in fact the small subunit of the protease otherwise referred to as CAPNS1 (*2*). In addition to calpains 1, 2, and 4, calpains 5, 7, 10, 12, and 13 are also ubiquitously expressed. While primarily cytosolic in nature, a proportion of some calpain isoforms have also been identified in specific subcellular organelles. Recent studies have shown that calpain 1 localizes between the inner and outer mitochondrial membrane (*16, 17*), while calpain 10 localizes to the matrix of the mitochondria (*18*), suggesting that compartmentalization might feature in the regulation of the ubiquitously expressed isoforms of these enzymes.

The remaining calpains (3, 6, 8, 9, and 11) have tissue-specific distributions (*2*). Calpain 3, initially referred to as p94, is the best studied of this group. It is a 94-kDa skeletal muscle-specific isoform of calpain that localizes to several regions of the sarcomere by binding the giant sarcomere protein, titin (*19*). It is thought that this interaction regulates the proteolytic activity of calpain 3 by sequestering the enzyme and helping to maintain it in an inactive form until required in the cell. To date, there are over 440 documented mutations in *CAPN3*, the gene encoding calpain 3, that cause limb-girdle muscular dystrophy type 2A (LGMD2A, OMIM 253600) (*10, 20*) (http://www.dmd.nl/CAPN3). LGMD2A is an autosomal recessive form of limb-girdle muscular dystrophy characterized by the gradual atrophy of muscles in the hip and shoulder areas: the limb-girdle. While many types of pathogenic mutations have been described, close to 50% are missense mutations (212 out of 440), many of which

[†] This research was funded by a grant to P.L.D. from the Canadian Institutes for Health Research. P.L.D. holds a Canada Research Chair in Protein Engineering. C.P.G. is the recipient of an NSERC PGSD3 scholarship, and R.A.H. was supported by an R. J. Wilson Fellowship and an Ontario Graduate Scholarship.

* To whom correspondence should be addressed. Phone: (613) 533-2983. Fax: (613) 533-2497. E-mail: peter.davies@queensu.ca.

[‡] Queen's University.

[§] Centre Hospitalier Universitaire Vaudois and University of Lausanne.

10.1021/bi900130u CCC: $40.75
Published on Web 02/18/2009

cause inactivation of the enzyme. It is hypothesized that loss or inactivation of calpain 3 leads to an accumulation of damaged and/or misfolded protein that impairs muscle structure or growth, causing atrophy and eventually LGMD2A (*21*). Besides proteolysis, calpain 3 may have additional functions, such as binding AHNAK or other proteins of the cytoskeleton, in addition to titin.

Hindering our ability to understand how these missense mutations cause LGMD2A is the lack of a three-dimensional structure of calpain 3. The full-length enzyme is inherently unstable *in vitro* due to its rapid autolytic degradation (*22*). However, based on its amino acid sequence similarity to both calpains 1 and 2 (54% and 51%, respectively), it is likely that calpain 3 adopts the same overall fold as the large subunit of the ubiquitously expressed isoforms of the enzyme. This consists of four domains (I−IV) with the proteolytic activity residing in the papain-like domains I and II. Heterodimerization of the enzyme occurs mainly via pairing of the penta-EF-hand (PEF)[1] domain IV of the large (80-kDa) subunit with the homologous PEF domain of the small (28-kDa) subunit.

The domain organization of calpain 3 is identical to that of the large subunits of calpains 1 and 2. However, this isoform has three additional sequences unique among the calpain family: NS, IS1, and IS2. IS1 and IS2 are different 48-residue insertion sequences present within domain II and in the linker between domains III/IV, respectively, while NS is a 52-residue N-terminal addition to the enzyme that takes the place of the anchor helix in calpain 2. Both NS and IS1 are cleaved intramolecularly, which is proposed to activate the enzyme (*23*), while IS2 appears to target the enzyme to titin in the sarcomere (*19*). Several naturally occurring splice variants of the protein have been identified that lack the NS, IS1, and/or IS2 sequences. Lp82 is a rodent lens-specific splice variant of calpain 3 lacking all three sequences (*24*). The human isoform of Lp82 is not expressed due to the accumulation of frame-shift mutations in the gene (*25*). However, studies have shown rodent Lp82 to be stable and enzymatically active in the lens, indicating a regulatory/localization role for the insertion sequences as opposed to a distinct structural role. Differentially regulated expression of additional calpain 3 isoforms lacking one or several of these unique elements during development or muscle maturation has also been observed (*26, 27*).

Also distinct to calpain 3 is its ability to homodimerize via its PEF domain IV (*28*). This is in contrast to calpains 1 and 2, which heterodimerize with the small subunit. While no definitive structural data exist for dimerization of the whole enzyme, recombinantly expressed isolated calpain 3 domain IV behaves as a dimer as indicated by both gel permeation chromatography and analytical ultracentrifugation (*29*). Modeling of a calpain 3 PEF domain IV homodimer based on the rat small subunit crystal structure indicated the dimerization interface is well conserved between the two, lending further support for the ability of p94 to homodimerize.

[1] Abbreviations: DTT, dithiothreitol; EDTA, ethylenediaminetetraacetic acid; FRET, fluorescence resonance energy transfer; HEPES, 4-(2-hydroxyethyl)-1-piperazineethanesulfonic acid; MW, molecular weight; PEF, penta-EF-hand; rfu, relative fluorescence units; RMSD, root mean square deviation; SDS−PAGE, sodium dodecyl sulfate−polyacrylamide gel electrophoresis; Tris, tris(hydroxymethyl)aminomethane.

Crystal structures of rat and human calpain 2 have been solved in the absence of Ca^{2+} (*30, 31*). Based on the high degree of sequence similarity between calpain 2 and calpain 3, the former structure was used as the template for a calpain 3 model in an attempt to understand and explain the significance of some of the missense mutations that cause LGMD2A (*32*). The model was successful in identifying some specific mutations located at points along the protein that might affect domain−domain interactions and disrupt alignment of the active site, thereby inactivating the enzyme and causing LGMD2A. However, this model of calpain 3 was based on a Ca^{2+}-free template, and as the crystal structure of the isolated proteolytic core has subsequently shown (*33*), there is a large interdomain rotation that occurs in the enzyme upon binding of Ca^{2+} ions that functions to align the active site of the protein.

Recently, the crystal structures of full-length rat calpain 2 bound by either the first or fourth inhibitory repeat of its endogenous inhibitor calpastatin were solved (*34, 35*). In addition to identifying a novel inhibitory mechanism, the active Ca^{2+}-bound conformation of the enzyme was revealed for the first time. There were very few changes in the structure of individual calpain domains. However, there were large shifts in the relative position and orientation of each domain within the protein. For example, the PEF domains moved closer to the proteolytic core of the enzyme and caused displacement of the N-terminal anchor helix, creating a more compact shape compared to its Ca^{2+}-free counterpart. Also, a basic loop located within domain III of the enzyme was found to interact with and stabilize the active site.

In this study, the recently solved Ca^{2+}-bound structures of calpain 2 have been used as a template for a Ca^{2+}-bound homodimeric model of calpain 3. This has allowed us to explain additional LGMD2A-causing missense mutations in the enzyme that were previously difficult to rationalize. Also, the modeling of calpain 3 in the Ca^{2+}-free state was revisited to accurately compare the apo and holo forms of the enzyme. Three regions of calpain 3 were identified that undergo a large conformational shift upon the binding of Ca^{2+}. These contain several amino acids that, when mutated, cause LGMD2A. The recombinant expression of full-length human calpain 3 in *Escherichia coli* has not been possible because of the enzyme's instability. However, some LGMD2A-causing mutations have been investigated by mutating the corresponding residues in rat calpain 2 (*32, 34*). Most recently, Moldoveanu et al. (*34*) replaced arginine residues located in and around the basic loop of domain III of calpain 2 with alanine to simulate mutations that cause LGMD2A. A significant decrease in activity of the mutants was observed along with an increase in Ca^{2+} requirement. Here we have made exact substitutions to match LGMD2A mutations in three different regions of the enzyme. The mutants analyzed in this study also demonstrate decreased enzyme activity. However, our data indicate the decrease in activity in all three regions is due, at least in part, to an increased rate of autolytic degradation of the enzyme.

MATERIALS AND METHODS

Homology Modeling of Calpain 3. The crystal structures of human calpain 2 (PDB 1KFU) and rat calpain 2 bound to rat calpastatin inhibitory repeat 4 in the presence of Ca^{2+}

(PDB 3BOW) were used as the templates for the Ca^{2+}-free and Ca^{2+}-bound calpain 3 models, respectively. Using the program PyMol (*36*), the large subunit (domains I−IV) of each template was duplicated and aligned via its PEF domain IV to the PEF domain IV of the second subunit along the lines of the domain IV/VI interaction in the heterodimeric calpain 2, thus creating a large subunit homodimer similar to that proposed by Ravulapalli et al. (*29*). The program Modeler (*37*) was used to model calpain 3. A structure-based alignment was created between calpain 3 and each subunit of the calpain 2 homodimer. This placed the NS, IS1, and IS2 sequences of calpain 3 into loop regions of the structural templates, allowing for their omission from the modeled calpain 3 structures. In particular, elimination of IS1 was accomplished by joining T273 to Y322 via a peptide bond, while IS2 was omitted by joining R592 to P641. The program Gromacs (*38*) was used for energy minimization. Each calpain 3 model was solvated in a cube with roughly 150000 water molecules and 18 Na^+ ions to neutralize the charge of the system. Following solvation, each model was energy minimized via steepest descents for ca. 400 steps or until convergence ($F_{max} < 1000$).

Construction, Expression, and Purification of Full-Length Rat Calpain 2 Mutants. Six different rat calpain 2 mutants (G423R, R417W, R628Q, T344M, D346E, and D362K) were made using the QuikChange site-directed mutagenesis kit (Stratagene) according to the manufacturer's protocol. Each of the six mutants was expressed and purified as previously described (*39*). Samples were analyzed for purity via 10% (w/v) SDS−PAGE in Tris−Tricine buffer followed by Coomassie brilliant blue staining.

FRET Kinetic Studies. Rat calpain 2 (either wild type or mutant) (50 nM) was used to digest 10 μM FRET-based substrate PLFAER (*40*) in 1 mL of buffer A (100 mM HEPES−HCl (pH 7.4), 1 mM DTT). $CaCl_2$ was added to a final concentration of 1 mM to initiate the reaction, and fluorescence was monitored as a function of time using a PerkinElmer LS-50-B fluorometer at an excitation wavelength of 335 nm and an emission wavelength of 505 nm. The rate of increase in fluorescence over the first 25 s after calcium addition was used to determine the initial activity. A total of three measurements were averaged to determine the activity of each mutant.

Autolysis Assay. Aliquots of purified rat calpain 2 (either wild type or mutant) (100 μg) were diluted into 200 μL of buffer A. Autolysis was initiated by addition of $CaCl_2$ to a final concentration of 1 mM. Aliquots (5 μg) were removed from the reaction at various time points (1, 2, 5, 10, 20, 40, and 60 min) and mixed with SDS loading buffer (62 mM Tris-HCl (pH 6.8), 2% (w/v) SDS, 10% glycerol, 14 mM β-mercaptoethanol, 0.01% (w/v) bromophenol blue, 25 mM EDTA) to stop the reaction. Aliquotted time points were heated at 95 °C for 5 min prior to analysis via 10% (w/v) SDS−PAGE. All gels were stained using Coomassie brilliant blue R-250.

RESULTS

Calpain 3 Model. We aligned calpain 3 to the human and rat calpain 2 large subunits using structure-based amino acid matching (Figure 1). The alignment shows a high degree of conservation throughout its length (52% identity, 71% similarity to both proteins) with the exception of the NS, IS1, and IS2 sequences. These three sequences, which are specific to calpain 3 and have no known structural homologues, were placed in solvent-exposed loop regions of the enzyme, allowing for their omission from both the Ca^{2+}-free and Ca^{2+}-bound models of calpain 3 without affecting their overall folds. Specifically, the 52 amino acid NS was omitted from the N-terminus of the protein, while the 48 amino acid IS1 was placed in a loop region between β-strands 2 and 3 of domain II, and the 48 amino acid IS2 was placed in the linker between domains III and IV.

Both the Ca^{2+}-free and Ca^{2+}-bound enzyme models homodimerize by association of their PEF domains (Figure 2). This interaction is almost identical to the domain IV/VI PEF interaction of calpain 2 in the Ca^{2+}-free and Ca^{2+}-bound states, respectively. There are no obvious steric hindrances to modeling calpain 3 as a homodimer via its PEF domain IV as the amino acids at the dimerization interface are well conserved, as can be seen in the alignment (Figure 1). The homodimerization of calpain 3 creates an enzyme with two active proteolytic sites located at opposite ends of the structure. This eliminates any obstruction of either active site from the opposite subunit as each subunit is aligned in an antiparallel manner as dictated by the nature of the PEF domain IV interaction.

Calpain 3 was originally shown to bind Ca^{2+} using $^{45}Ca^{2+}$ gel overlay experiments, and its autolytic degradation was also demonstrated to be Ca^{2+}-dependent (*41*). We predict calpain 3 binds Ca^{2+} in the same manner as rat calpain 2. We note that the overall amino acid conservation between the two proteins is 52% but that there is 96% conservation of Ca^{2+}-coordinating residues between the two proteins (Figure 1). Our Ca^{2+}-bound model of calpain 3 binds 12 Ca^{2+} ions in total, with 6 in each individual subunit. The proteolytic core (domains I−II) binds 2 Ca^{2+} ions in order to align the active site, while the PEF domain IV binds 4 Ca^{2+} ions. We predict calpain 3 to be a homodimer in the Ca^{2+}-free and Ca^{2+}-bound states. This is based on the previous work by Ravulapalli et al. (*29*), where recombinantly expressed isolated calpain 3 PEF domain IV was shown via both gel permeation chromatography and analytical ultracentrifugation to be a homodimer in the presence of either Ca^{2+} or EDTA.

We assessed the stereochemical quality of each calpain 3 model using the program Procheck (*42*). Both the Ca^{2+}-free and Ca^{2+}-bound models had greater than 97% of their residues fall within allowable regions of the Ramachandran plot, indicating high-quality models (data not shown). The Ca^{2+}-bound and Ca^{2+}-free models of calpain 3 match very closely with their structural templates. The α-carbon RMSD of calpain 3 to the rat Ca^{2+}-bound and human Ca^{2+}-free structural templates after energy minimization was 0.25 and 0.56 Å, respectively, while the Ca^{2+}-bound and Ca^{2+}-free models of calpain 3 have an α-carbon RMSD of 9.15 Å when aligned to each other over the entire length of their sequence. This large difference is the result of the major reorientation of each individual domain of the enzyme upon the binding of Ca^{2+}. In particular, all of the major changes observed upon the binding of Ca^{2+} by rat calpain 2 are mimicked by calpain 3. There is a large rotation of domain II in relation to domain I that aligns the active site of the enzyme. This rotation, in turn, causes a rotation of the C2-like domain III

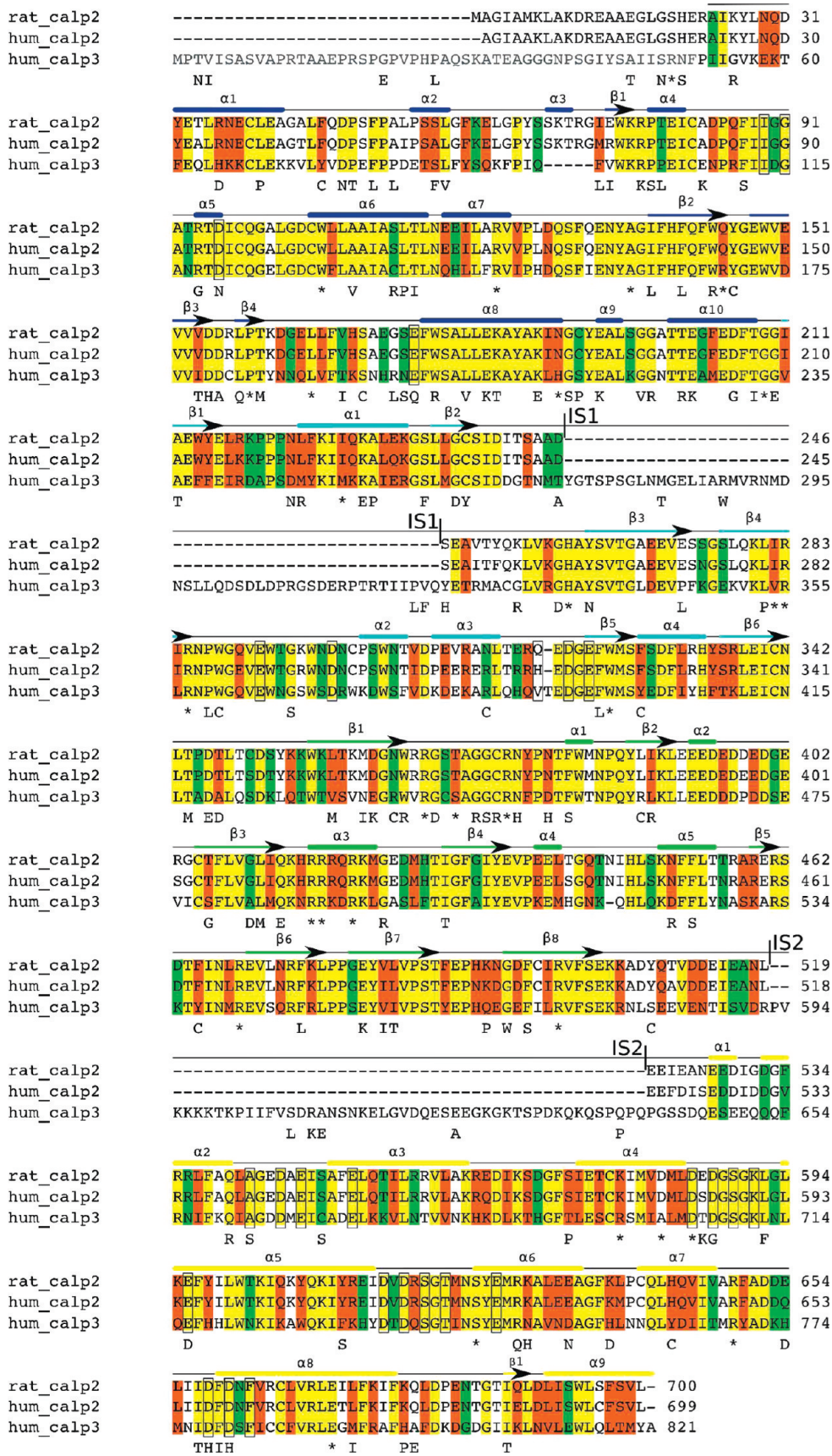

FIGURE 1: Structure-based amino acid alignment of calpains. Secondary structure elements (α = α-helix, β = β-strand) of the Ca^{2+}-bound rat calpain 2 crystal structure are numbered sequentially above the sequence and are colored according to individual domains (blue = I, light blue = II, green = III, yellow = IV). Identical residues between the three proteins are highlighted in yellow. Conserved substitutions are highlighted in orange. Semiconserved substitutions are highlighted in light green. Ca^{2+}-binding residues are boxed in black. Gray residues at the beginning of the alignment represent NS from calpain 3 and are not aligned to the template sequences due to lack of homology. The boundaries of IS1 and IS2 are indicated by vertical lines. Calpain 3 residues that undergo mutation to cause LGMD2A are indicated by the corresponding mutated residue below the alignment. An asterisk indicates a residue that can undergo multiple mutations to cause LGMD2A.

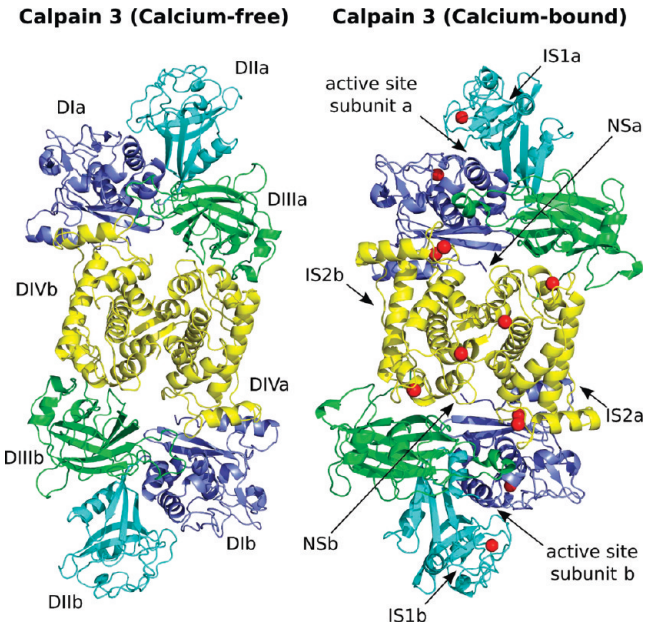

FIGURE 2: Ca^{2+}-free and Ca^{2+}-bound homodimeric models of calpain 3. Calpain 3 was modeled as a homodimer in both the Ca^{2+}-free and Ca^{2+}-bound form by association of the PEF domain IV from each subunit. Domains are colored as follows: I = blue, II = light blue, III = green, and IV = yellow. Ca^{2+} ions are indicated by red spheres. Arrows point to the theoretical locations of NS, IS1, and IS2, as well as the active site for both subunits of the Ca^{2+}-bound model. a = subunit a of the calpain 3 homodimer, while b = subunit b of the calpain 3 homodimer.

away from domain II and forward (relative to the view of subunit a in Figure 2) over domain IV. Domain IV is translated closer to domain I. All of these movements are easily accommodated in the Ca^{2+}-bound model of calpain 3 and create a more compact structure as compared to its Ca^{2+}-free counterpart.

As previously mentioned, there are currently over 440 mutations in the calpain 3 gene that are known to cause LGMD2A, more than half of which are single amino acid substitutions that can destroy or severely impair the proteolytic activity of calpain 3. These mutations are evenly spread out across the length of the protein. By mapping their locations on both the Ca^{2+}-bound and Ca^{2+}-free models of calpain 3, the majority of these mutations were observed to be in sites of the protein that do not undergo a conformational change upon the binding of Ca^{2+} and therefore are explainable with either a Ca^{2+}-free or Ca^{2+}-bound model of calpain 3. However, a close comparison of the two models revealed three distinct areas of the protein that undergo a large conformational change upon the binding of Ca^{2+}: (1) the linker connecting domains II and III, (2) the basic loop connecting β-strands 3 and 4 of domain III, and (3) the interface between domains III and IV. These three areas will be discussed in detail below as will the corresponding rat calpain 2 mutants that were created to investigate their effects *in vitro*.

Domain II/III Linker Region. There is a 15 amino acid loop (residues 415−429) that connects domain II to domain III in calpain 3 (colored pink in Figure 3) in which the LGMD2A mutations T417M, D419E, and A420D are found. In the Ca^{2+}-free model, T417 and A420 are solvent-exposed while the side-chain carbonyl oxygen of D419 hydrogen bonds with the side-chain amide nitrogen of N415, the first residue in the loop (Figure 3A). Upon the binding of Ca^{2+} to the protein, a major reorientation of the loop occurs. The loop swings down and away from domains I and II (relative to the view in Figure 3) and toward domain II/III. In particular, when the Ca^{2+}-free and Ca^{2+}-bound models are aligned to one another by their respective domain II's, the α-carbon of T417 moves 6.7 Å down and away from its original position, while the α-carbons of D419 and A420 move 15.1 and 18.8 Å, respectively, from their original position behind the active site of the protein and toward different regions of domains II and III (Figure 3B). In this new position, the side-chain hydroxyl group of T417 hydrogen bonds with a side-chain carbonyl oxygen of D419, which itself is hydrogen bonded to the indole nitrogen of W429. The main-chain carbonyl oxygen of A420 hydrogen bonds with the main-chain nitrogen of S423.

This 15 amino acid loop connecting domain II to domain III appears to allow for the proper rotation of these two neighboring domains while at the same time stabilizing their new orientation as several of the other residues in the loop make both ionic and van der Waals contacts with both domains II and III (Figure 3B). These include the side-chain hydrogen bond between K425 and D472, as well as an extensive hydrogen-bonding network between S260, N415, E237, L421, A420, and S423. All three of the T417M, D419E, and A420D LGMD2A mutations would appear to be well tolerated in the Ca^{2+}-free form of calpain 3. T417 and A420 are each solvent exposed with no particular neighbor interactions while the D419E mutation should be easily accommodated as the nature of the D and E side chains are the same and therefore still able to hydrogen bond with N415 (Figure 3A). However, in the Ca^{2+}-bound form of calpain 3, the length of the side chain of D419 appears critical to form hydrogen bonds to the side chains of T417 and W429. Mutation to the longer glutamate side chain would eliminate this interaction and destabilize the loop. The same can be said for the side chain of T417. Mutation to a Met residue would eliminate its ability to hydrogen bond with D419 and therefore destabilize the loop. The significance of the A420D mutation is still not fully understood as A420 hydrogen bonds with S423 via its main-chain, not side-chain, carbonyl oxygen. It is possible however, that the negative charge of the Asp side chain could disrupt the orientation of the loop in the Ca^{2+}-free form.

We created the T417M (T344M) and D419E (D346E) mutations in rat calpain 2 (corresponding rat calpain 2 mutant site in parentheses). Each mutant enzyme was purified to homogeneity, and their total yields were determined to be 60% and 40% of wild-type yields, respectively (Table 1). The proteolytic activity of each mutant in comparison to the wild type was determined by measuring their relative ability to cleave the FRET-based PLFAER peptide. Cleavage of the peptide results in the relief of fluorescence quenching, causing a measurable increase in fluorescence as a function of time. The T344M and D346E mutants had only roughly 30% and 55% of initial wild-type activity, respectively (Table 1). Also, each mutant lost the ability to hydrolyze the PLFAER peptide approximately 3.5× faster than wild type (500 s for both T344M and D346E vs 1800 s for wild type), as demonstrated by their earlier plateau of fluorescence in Figure 4. Since calpain is known to autolyze in the presence of excess Ca^{2+}, our data suggest that the T344M and D346E

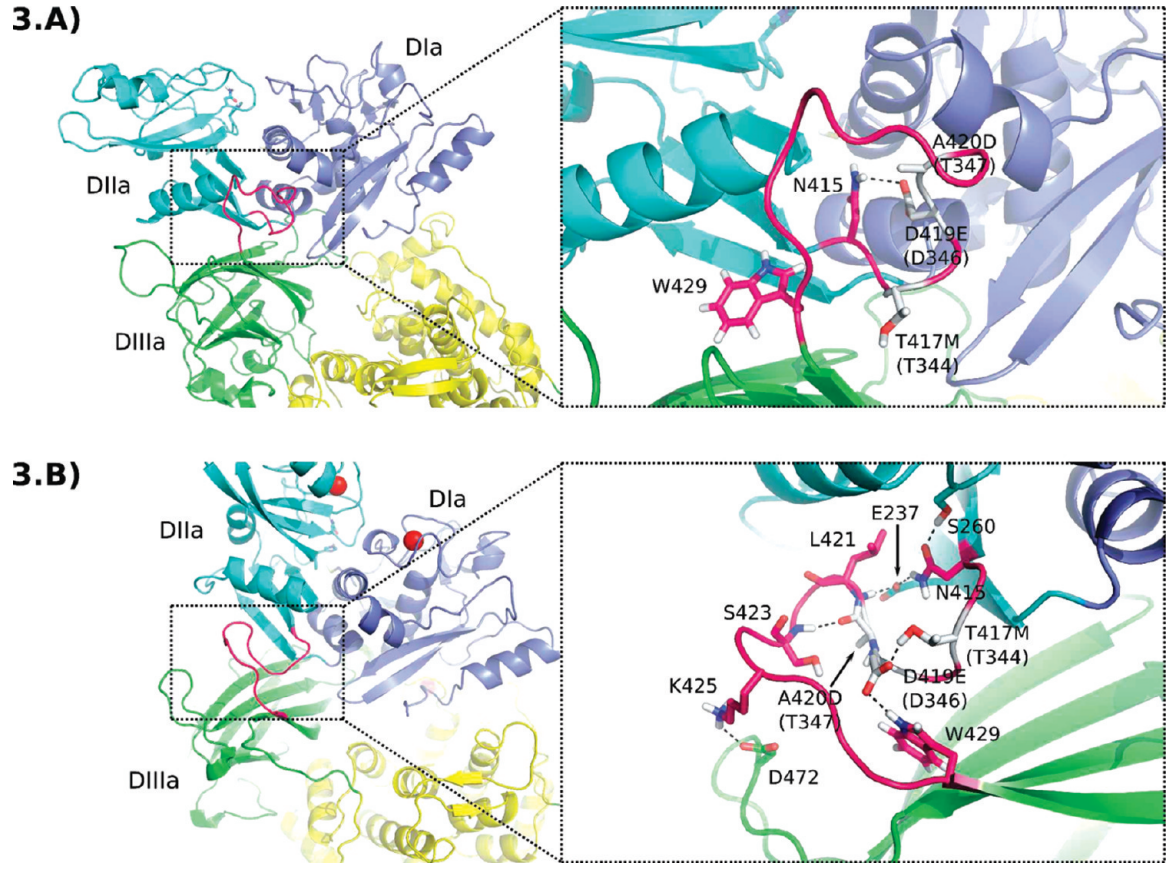

FIGURE 3: Domain II/III linker. Ca^{2+}-free (A) and Ca^{2+}-bound (B) models of calpain 3 highlighting the 15-aa loop (colored magenta) that connects domain II to domain III. The three LGMD2A-causing mutations (T417M, D419E, A420D) located in this loop are shown in their nonmutated forms and are colored in white, except for O atoms (red) and N atoms (blue). Hydrogen bonds between atoms are indicated by black dashed lines. Other residues in the domain II/III linker that play critical roles in the correct orientation and stabilization of the loop are colored in magenta. Residues that interact with but are located outside of the domain II/III linker are colored according to their domain of origin as described in Figure 2.

Table 1: Yield and Average Initial Activity for Wild-Type and Mutant Calpain 2 Enzymes

calpain 2 mutation[a]	corresponding position in calpain 3	yield (mg of protein/L of *E. coli* culture)	av initial rate (rfu/s)
wild type		5	1.3 ± 0.1
G423R (basic loop)	G496	4	0.84 ± 0.04
R417W (basic loop)	R490	3	N/A
R628Q (domain III/IV interface)	R748	3	0.19 ± 0.01
T344M (domain II/III linker)	T417	3	0.36 ± 0.02
D346E (domain II/III linker)	D419	2	0.7 ± 0.4
D362K (domain III/IV interface)	E435	1	1.0 ± 0.3

[a] Mutation location in parentheses.

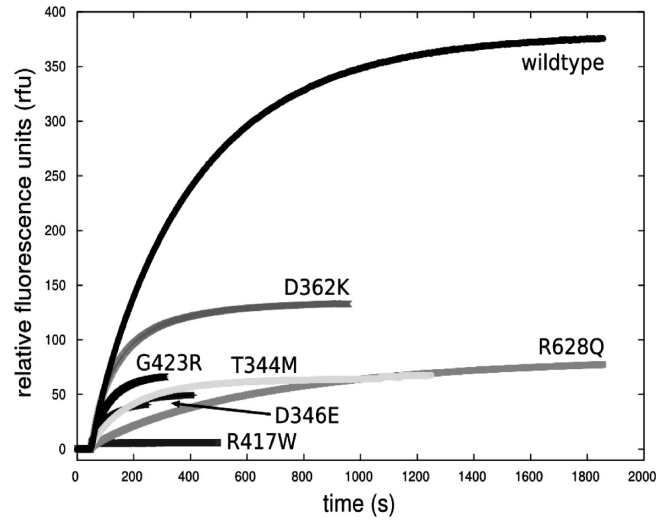

FIGURE 4: Hydrolysis of FRET-based PLFAER peptide. Catalytic activity of wild-type and mutant calpain 2 enzymes was monitored by cleavage of the (EDANS)−PLFAER−(DABCYL) peptide, resulting in the relief of fluorescence quenching (*40*). Relative fluorescence units (rfu) vs time (s) is plotted for each enzyme.

mutants might be autolyzing at a faster rate as compared to wild type. We therefore monitored the autolysis of both wild-type and mutant calpain 2 enzymes in the presence of excess Ca^{2+} via SDS−PAGE.

The autolysis profile of wild-type calpain 2 is shown in Figure 5A. Two distinct bands are visible at the 0 time point control (no Ca^{2+} added), one at 80 kDa and the other at 21 kDa. These bands correspond to the large and small subunits of calpain 2, respectively. Upon Ca^{2+} addition, the enzyme began to autolyze as can be seen by the decreased intensity of the 80-kDa and, to a lesser extent, the 21-kDa subunits and the appearance of several intermediate bands. These include one at ~50 kDa, another at ~40 kDa, and four others between 20 and 26 kDa. The autolysis profile of the T344M mutant revealed a much faster rate of autolysis as compared to wild type, as evidenced by the almost complete disappearance of the large 80-kDa band after 20 min (Figure 5B). The amount of residual 80-kDa subunit in T344M after 10 min is equivalent to the amount left in the wild type after

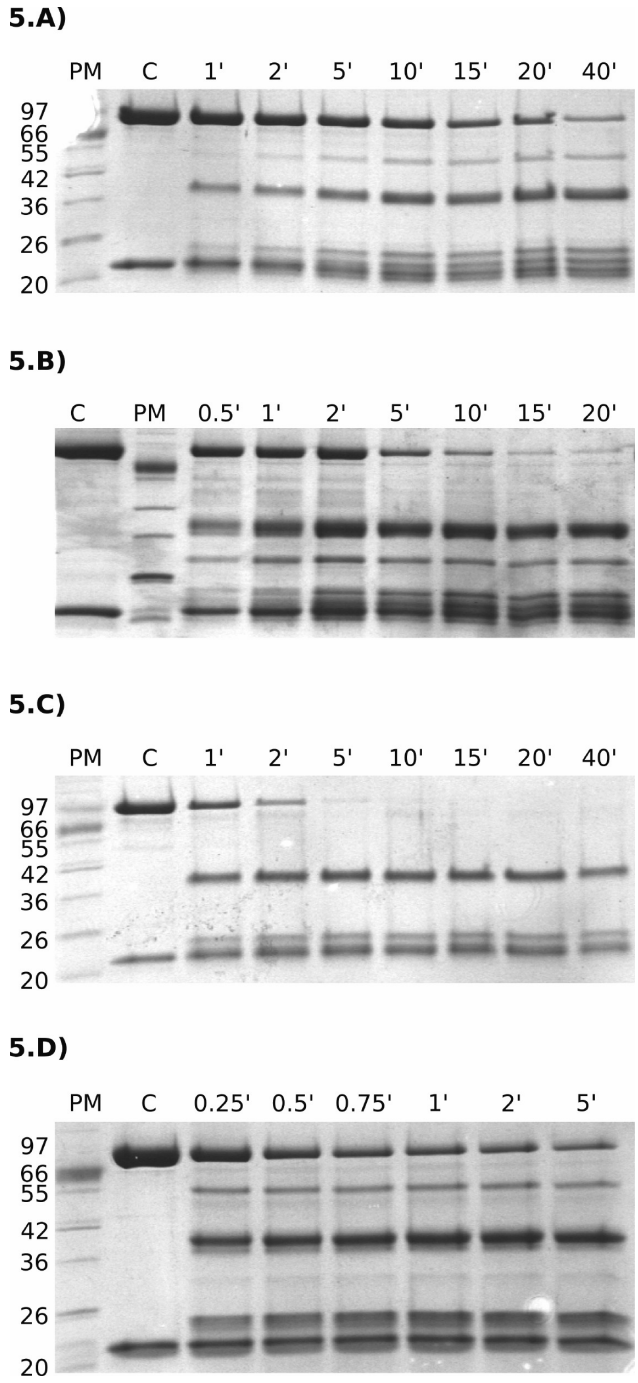

FIGURE 5: SDS−PAGE analysis of selected rat calpain 2 mutants. The autolysis profile of wild-type calpain 2 is shown in panel A. PM = protein markers; C = control (no added Ca^{2+}). Numbers above each lane of the (10% w/v) SDS−PAGE gel represent individual time points (min) of the assay. The MW ($\times 10^{-3}$) of each protein standard is shown down the left-hand side of the gel. Equal amounts of protein (5 μg) were applied in each lane. The autolysis profile of the T344M calpain 2 mutant is shown in panel B, while the autolysis profiles of the G423R and R417W calpain 2 mutants are shown in panels C and D, respectively.

40 min. Also, the 50-kDa band visible on the wild-type profile after 1 min and which intensifies throughout the course of the digestion is much fainter in the T344M autolysis profile and disappears completely after 15 min. A novel band is seen in the T344M autolysis profile at roughly 30 kDa that is not seen in the wild-type profile. A similar autolysis profile was observed for the D346E mutant (data not shown). Taken together, both the fluorescence and autolysis data indicate the T344M and D346E mutations cause calpain 2 autolysis to proceed at an increased rate as compared to wild type, resulting in premature inactivation of the enzyme.

Basic Loop of Domain III. A 15 amino acid loop (residues 487−501) connects β-strands 2 and 3 of domain III in calpain 3 (colored pink in Figure 6). The mutations R489W/Q, R490W/Q, R493G/Q, and G496R all locate to this loop and cause LGMD2A. This loop is positioned just underneath the active site of the enzyme in both the Ca^{2+}-free and Ca^{2+}-bound models of calpain 3; however, its conformation is radically different depending upon the Ca^{2+}-binding state of the enzyme. In the Ca^{2+}-free model, the loop is unstructured and the side chains of R489, R490, and R493 point away from the active site (Figure 6A). In particular, the side chain of R489 hydrogen bonds with the side-chain carbonyl oxygen of E568 (located in β-strand 8 of domain III). R490 hydrogen bonds with what will become the four Ca^{2+}-binding residues of the second EF hand of domain IV of the opposite subunit. These include the side-chain carbonyl oxygens of E667, D705, and D707, as well as the main-chain carbonyl oxygen of K711. R493 hydrogen bonds with the side-chain carbonyl oxygen of D665 (itself a Ca^{2+}-coordinating residue in the first EF hand of domain IV of the opposite subunit) as well as the main-chain carbonyl oxygens of R490 and K491 (not shown). Finally, G496 provides flexibility to the loop as it adopts main-chain ϕ/ψ angles only allowable for Gly residues. Upon the binding of Ca^{2+} to the enzyme, residues 489−495 in the 15 amino acid loop adopt an α-helical conformation with the side chains of both R490 and R493 pointing toward the bottom of the active site of the enzyme (Figure 6B). In particular, R490 hydrogen bonds with the main-chain carbonyl oxygens of A218 and L219, both located in a loop right below the active site cysteine (C129). R490 also hydrogen bonds with the side-chain carbonyl oxygen of E226, located in helix 10 of domain I which is itself a residue whose mutation to a Lys causes LGMD2A. R493 interacts with the main-chain carbonyl oxygen atoms of both K220 and G221, each of which is located in the same loop that contains A218 and L219, while R489 interacts with the main-chain carbonyl oxygen of S498 and the side-chain carbonyl oxygen of D492.

This 15 amino acid loop appears to play a critical role in the stability of both the Ca^{2+}-free and Ca^{2+}-bound structures of calpain 3. In the Ca^{2+}-free model, this loop has key contacts with both domain III and domain IV from the opposite subunit of the calpain 3 pair, all of which helps to stabilize the fold of the dimer. The binding of Ca^{2+} by domain IV would then displace both R490 and R493 from EF hands 1 and 2 of the opposite subunit and allow them to adopt an α-helical conformation that points their side chains toward the cysteine of the active site, helping to stabilize this area. The short helix appears to be stabilized by the side chain of R489 which interacts with D492, via an i, $i + 3$ salt bridge, and S498 (both residues within the Ca^{2+}-induced helix) instead of E568 from domain III.

The corresponding R490W (R417W) and G496R (G423R) mutations were created in rat calpain 2, and the mutated enzymes were purified to homogeneity. Their respective yields were 60% and 80% of wild type (Table 1). The G423R mutant had approximately 65% of initial wild-type activity, and that activity terminated roughly 6× faster (plateau in

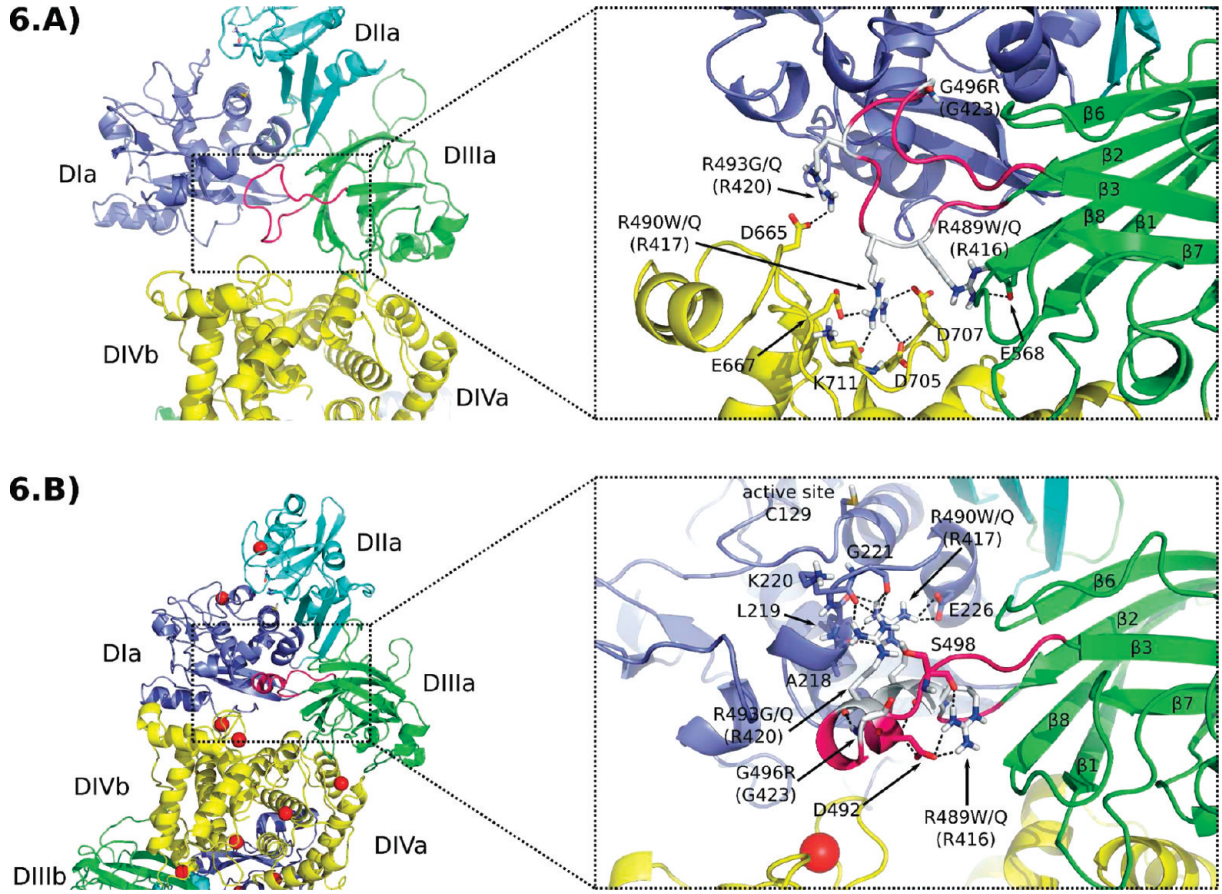

FIGURE 6: Domain III basic loop. Ca^{2+}-free (A) and Ca^{2+}-bound (B) models of calpain 3 highlighting the 15-aa loop (colored in magenta) that connects β-strands 2 and 3 in domain III. The four LGMD2A-causing mutations (R489WQ, R490WQ, R493GQ, G496R) located in this loop are shown in their nonmutated forms and are colored in white. Other details are as described in the legend to Figure 3.

fluorescence at 300 s vs 1800 s for wild type) (Figure 4). The autolysis profile of the G423R mutant showed a rapid degradation of the 80-kDa large subunit. The amount of residual 80-kDa subunit in G423R after 2 min is equivalent to the amount left in wild type after 40 min, and the band completely disappears after only 5 min (Figure 5C). Also, there were fewer bands located between the 20−26-kDa size range as compared to wild type, and there was no 50-kDa band visible at any time point on the G423R profile as was seen on the wild-type profile. Like the T344M and D346E mutants, these data indicate the G423R mutant undergoes autolysis at an increased rate as compared to wild type, and this lowers the effective amount of enzyme capable of proteolyzing target substrate.

The R417W mutant showed no cleavage of the PLFAER peptide as no increase in fluorescence was observed upon Ca^{2+} addition (Figure 4). Interestingly, the SDS−PAGE autolysis profile of the R417W mutant (Figure 5D) showed an extremely rapid partial digestion of the large 80-kDa subunit of the enzyme immediately upon Ca^{2+} addition. However, there was no change in the banding pattern after about 1 min, indicating no further autolysis. Both the large (80-kDa) and small (21-kDa) subunits of the enzyme were still present throughout the time course though, as were bands at roughly 50 and 40 kDa and approximately four bands present between the 20−26-kDa range. This mutation caused an extremely rapid partial degradation of the enzyme which was then rendered totally inactive.

Domain III/IV Interface. Located at an interior interface between domains III and IV of calpain 3 are the LGMD2A mutations E435K, R437C, and R748Q (Figure 7). Both E435 and R437 are located in the first β-strand of domain III while R748 is located in the second α-helix of PEF-3 of domain IV. In the Ca^{2+}-free model of calpain 3, E435 has no binding partners and is solvent exposed, while the side chain of R437 hydrogen bonds with the side-chain carbonyl oxygen of E568 (located in the eighth β-strand of domain III), and the side chain of R748 hydrogen bonds with the side-chain carbonyl oxygen of E585 (located in the linker between domains III and IV) (Figure 7A). After Ca^{2+} binding, the new orientation of domain III with respect to domain IV is stabilized in part by an extensive salt bridge network at their interior interface involving E435, R437, and R748 (Figure 7B). In this network, the side chain of E435 hydrogen bonds with the side-chain amino nitrogen of K487 (located in a loop region between β-strand 3 and α-helix 3 of domain III) and the side-chain amino nitrogen of N760 (located in the first α-helix of PEF-4 in domain IV). Also within this network, the side chain of R748 hydrogen bonds to both the main-chain and side-chain carbonyl oxygens of D764 (located in the same helix as N760) which is itself hydrogen bonded to K487. The movement of domain III with respect to domain IV also allows for the side chain of R437 to interact with the main-chain carbonyl oxygen of K773 while maintaining its original interaction with the side chain of E568.

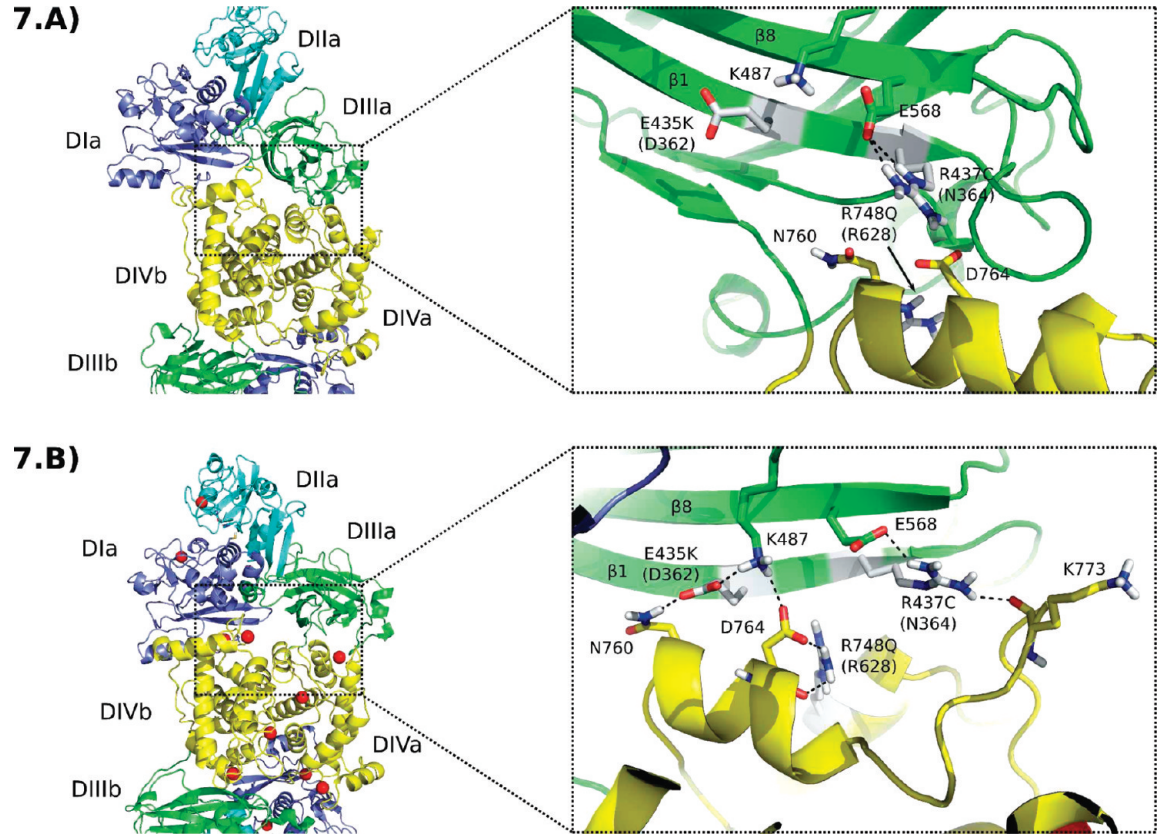

FIGURE 7: Domain III/IV interface. Ca^{2+}-free (A) and Ca^{2+}-bound (B) models of calpain 3 highlighting the interface between domains III and IV. The three LGMD2A-causing mutations (E435K, R437C, R748Q) located in this region are shown in their nonmutated forms and are colored in white. Other details are as described in the legend to Figure 3.

The corresponding E435K (D362K) and R748Q (R628Q) mutations were made in rat calpain 2. After purifying the enzymes to homogeneity, their respective yields were 20% and 60% of wild type (Table 1). The R628Q mutant had only ~15% of wild-type activity based on initial reaction rates (Table 1). While R628Q digested the PLFAER peptide at a much slower rate as compared to the wild type, it maintained the ability to hydrolyze the peptide over the entire course of the experiment, as a plateau in fluorescence was approached but not reached (Figure 4). The autolysis profile of the R628Q mutant (data not shown) was qualitatively identical to the wild-type autolysis profile with respect to the fragments generated and the time over which they were generated. In particular, a gradual decrease in the intensity of the bands corresponding to the large and small subunits of the enzyme was observed, as was a corresponding increase in the number and intensity of bands representing smaller breakdown products of the enzyme. These data indicate that the R628Q mutation did not increase the rate of autolysis of the enzyme but was able to hinder the enzyme's ability to hydrolyze target substrate. This was the only mutant generated in this study for which this phenomenon was observed.

The D362K mutant had roughly 75% of initial wild-type activity (Table 1). It lost the ability to hydrolyze the PLFAER mutant after ~500 s, which, like the T344M and D346E mutants, was approximately 3−4 times sooner than with the wild type (Figure 4). The autolysis profile of the D362K mutant (data not shown) was essentially identical to that of both the T344M and D346E mutants. There was almost complete disappearance of the large subunit band after 20 min, a rapid degradation of the ~50-kDa band after 15 min, and the appearance of a ~30-kDa band not seen in the wild-type profile. Taken together, these data indicate the D362K mutation accelerates autolytic degradation and thereby lowers the amount of active enzyme capable of proteolyzing substrates.

DISCUSSION

All six calpain 2 mutants examined in this study had lower activity levels as compared to the wild type, and all but one (R628Q) were found to have increased rates of autoproteolytic degradation. It is not clear that the decreased enzyme activity is simply a result of increased autoproteolysis, because these mutations might also affect the alignment of, or access to, the active site of the enzyme. The R417W mutant, for example, was found to have an extremely rapid autoproteolytic degradation followed by complete inactivation of the enzyme, as is evident by the lack of change in Coomassie blue-stained fragments following the initial proteolytic cleavages at the 15 s time point. This would seem to indicate the mutation not only increases susceptibility to autoproteolysis but also distorts the active site of the enzyme, rendering it unable to cleave substrates. It might also indicate that there is a folding dichotomy within the R417W population, undetectable during the course of purification, where some fraction of the protein is capable of autoproteolysis and the remaining fraction is inactive. The inability of R417W to cleave the PLFAER peptide also highlights the increased autoproteolytic nature of the mutant enzyme, as any functioning enzyme was quickly autoproteolyzed and rendered unable to cleave potential substrate.

A large difference was observed between the activity of the R417W calpain 2 mutant made in this study and the R417A calpain 2 mutant examined by Moldoveanu et al. (*34*). A 50% decrease in activity was seen with R417A, while a complete abrogation of activity was observed for R417W. R417 plays a critical role in the stabilization of the active site of calpain 2, as indicated by the extensive hydrogen bonding of its side-chain guanidino group to several residues in its vicinity. Mutating R417 to Ala would eliminate those stabilizing hydrogen bonds and therefore cause a decrease in activity, as was observed. However, the R417W mutation (a naturally occurring LGMD2A-causing mutation) examined in this study would not only eliminate those key stabilizing interactions but would also significantly distort the active site due to the bulky, hydrophobic nature of the Trp side chain, therefore resulting in much lower activity levels. Also, R417 interacts with several Ca^{2+}-binding residues located in EF-hand 2 of the opposite subunit. How the R417W mutation would affect these contacts and the implications for folding of the enzyme in the inactive state are unknown.

The R628Q mutant was the only enzyme that did not undergo an observable change in the rate of autoproteolysis, even though its activity was only 15% of wild type. This result is in contrast to that of the D362K mutation (located in the same area of the domain III/IV interface) that had a much higher activity level (75% of wild type) but also an increased autoproteolytic rate. It is not clear at this time how these two mutations in the same region can produce such drastically different results.

The exact locations of the autoproteolytic sites of both the wild-type and mutant calpain 2 enzymes are unknown. Significant differences were observed in the SDS−PAGE banding pattern between the wild-type and mutant enzymes as well as between individual mutants themselves. This indicates different areas of the enzyme are rendered more or less susceptible to autoproteolysis based on the type and location of a specific mutation. It would seem reasonable to predict that point mutations in both the domain II/III linker region and the basic loop of domain III would make these areas more susceptible to autoproteolytic degradation due to decreased stability and increased disorder of those regions. This in turn could produce novel band(s) visible by SDS−PAGE. However, there is a high probability that a mutation will also affect the ability of the enzyme to cleave a potential substrate (either itself or another target) as was the case with the R417W mutant (unable to cleave the PLFAER substrate, rapid and abrupt termination of autoproteolysis). Therefore, just because a mutation could make an area more susceptible to proteolysis does not mean it will necessarily be cut.

All calpain 2 mutations produced in this study had detrimental effects on calpain activity. On the basis of modeling, we predict the corresponding mutations in calpain 3 would have the same deleterious effects on enzyme activity. Whether through increased autoproteolysis or decreased enzyme activity, the putative *in vivo* effect of these mutations would be decreased target substrate proteolysis. One of the main roles of calpain 3 *in vivo* is to eliminate damaged sarcomeric proteins that, if left untreated, can compromise the integrity of the sarcomere itself and eventually lead to loss of muscle contraction (*21*). Any of the mutant enzymes from this study would be unable to perform this task, therefore resulting in LGMD2A.

Calpain 3 has been shown to interact with titin in the sarcomere through IS2 (*43, 44*). This interaction is predicted to maintain the enzyme in an inactive state, incapable of autoproteolysis, but in close proximity to potential substrates. While not modeled in this study due to a lack of homologues, IS2 would theoretically extend from opposite sides of the homodimeric enzyme. This would allow calpain 3 to bind titin in one of three different ways: (1) a single IS2 sequence from one calpain 3 subunit binding to a single titin molecule; (2) both IS2 sequences from the calpain 3 dimer binding to a single titin molecule; (3) both IS2 sequences from the dimer binding to two adjacent titin molecules. It would seem reasonable to predict that both IS2 sequences of the calpain 3 homodimer would need to be sequestered by titin to prevent activation of the enzyme. Therefore, binding to two adjacent titin molecules is an intriguing hypothesis as it would maintain calpain 3 completely inactive but allow it to respond to changes in the integrity of the sarcomere. Several proteins of the sarcomere, especially titin, are susceptible to shear forces during muscle use due simply to their extreme length. Once sheared, the local disorganization of the sarcomere lattice structure increases, allowing for greater mobility of proteins in the immediate vicinity. Therefore, once damage has occurred, calpain 3 could be activated by elevated Ca^{2+} levels (*45*) with release from titin to perform its proteolytic duties in the area of the damage. Much work remains to be done, however, in identifying substrates of calpain 3 in the sarcomere in order to validate this hypothesis.

In conclusion, we have modeled the muscle-specific human calpain 3 enzyme using the recently solved Ca^{2+}-bound rat m-calpain/calpastatin crystal structure. This identified three areas in the enzyme that undergo a large conformational change upon the binding of Ca^{2+}. Present within those areas are several residues that, when mutated, cause LGMD2A. By making the corresponding mutations in rat calpain 2, a significant decrease in enzyme activity was observed for all mutants created; however, for the majority of mutants tested, the decrease in activity was the result of an increased rate of autoproteolytic degradation of the enzyme.

REFERENCES

1. Guroff, G. (1964) A neutral, calcium-activated proteinase from the soluble fraction of rat brain. *J. Biol. Chem. 239*, 149–155.
2. Goll, D. E., Thompson, V. F., Li, H., Wei, W., and Cong, J. (2003) The calpain system. *Physiol. Rev. 83*, 731–801.
3. Glading, A., Lauffenburger, D. A., and Wells, A. (2002) Cutting to the chase: calpain proteases in cell motility. *Trends Cell. Biol. 12*, 46–54.
4. To, K. C., Church, J., and O'Connor, T. P. (2008) Growth cone collapse stimulated by both calpain- and Rho-mediated pathways. *Neuroscience 153*, 645–653.
5. Santella, L. (1998) The role of calcium in the cell cycle: facts and hypotheses. *Biochem. Biophys. Res. Commun. 244*, 317–324.
6. Cheng, Y., Qiu, F., Huang, J., Tashiro, S. I., Onodera, S., and Ikejima, T. (2008) Apoptosis-suppressing and autophagy-promoting effects of calpain on oridonin-induced L929 cell death. *Arch. Biochem. Biophys. 475*, 148–155.
7. Dale, Y. R., and Eltom, S. E. (2006) Calpain mediates the dioxin-induced activation and down-regulation of the aryl hydrocarbon receptor. *Mol. Pharmacol. 70*, 1481–1487.
8. Horikawa, Y., Oda, N., Cox, N. J., Li, X., Orho-Melander, M., Hara, M., Hinokio, Y., Lindner, T. H., Mashima, H., Schwarz, P. E., del Bosque-Plata, L., Horikawa, Y., Oda, Y., Yoshiuchi, I., Colilla, S., Polonsky, K. S., Wei, S., Concannon, P., Iwasaki, N., Schulze,

J., Baier, L. J., Bogardus, C., Groop, L., Boerwinkle, E., Hanis, C. L., and Bell, G. I. (2000) Genetic variation in the gene encoding calpain-10 is associated with type 2 diabetes mellitus. *Nat. Genet. 26*, 163–715.
9. Ridderstråle, M., and Nilsson, E. (2008) Type 2 diabetes candidate gene CAPN10: first, but not last. *Curr. Hypertens. Rep. 10*, 19–24.
10. Kramerova, I., Beckmann, J. S., and Spencer, M. J. (2007) Molecular and cellular basis of calpainopathy (limb girdle muscular dystrophy type 2A). *Biochim. Biophys. Acta 1772*, 128–144.
11. Lee, M. S., Kwon, Y. T., Li, M., Peng, J., Friedlander, R. M., and Tsai, L. H. (2000) Neurotoxicity induces cleavage of p35 to p25 by calpain. *Nature 405*, 360–364.
12. Raynaud, F., and Marcilhac, A. (2006) Implication of calpain in neuronal apoptosis. A possible regulation of Alzheimer's disease. *FEBS J. 273*, 3437–3443.
13. Tang, Y., Liu, X., Zoltoski, R. K., Novak, L. A., Herrera, R. A., Richard, I., Kuszak, J. R., and Kumar, N. M. (2007) Age-related cataracts in alpha3Cx46-knockout mice are dependent on a calpain 3 isoform. *Invest. Ophthalmol. Visual Sci. 48*, 2685–2694.
14. Sakamoto-Mizutani, K., Fukiage, C., Tamada, Y., Azuma, M., and Shearer, T. R. (2002) Contribution of ubiquitous calpains to cataractogenesis in the spontaneous diabetic WBN/Kob rat. *Exp. Eye Res. 75*, 611–617.
15. Schaecher, K., Rocchini, A., Dinkins, J., Matzelle, D. D., and Banik, N. L. (2002) Calpain expression and infiltration of activated T cells in experimental allergic encephalomyelitis over time: increased calpain activity begins with onset of disease. *J. Neuroimmunol. 129*, 1–9.
16. Kar, P., Chakraborti, T., Samanta, K., and Chakraborti, S. (2008) Submitochondrial localization of associated mu-calpain and calpastatin. *Arch. Biochem. Biophys. 470*, 176–186.
17. Badugu, R., Garcia, M., Bondada, V., Joshi, A., and Geddes, J. W. (2008) N terminus of calpain 1 is a mitochondrial targeting sequence. *J. Biol. Chem. 283*, 3409–3417.
18. Arrington, D. D., Van Vleet, T. R., and Schnellmann, R. G. (2006) Calpain 10: a mitochondrial calpain and its role in calcium-induced mitochondrial dysfunction. *Am. J. Physiol. Cell Physiol. 291*, C1159−1171.
19. Hayashi, C., Ono, Y., Doi, N., Kitamura, F., Tagami, M., Mineki, R., Arai, T., Taguchi, H., Yanagida, M., Hirner, S., Labeit, D., Labeit, S., and Sorimachi, H. (2008) Multiple molecular interactions implicate the connectin/titin N2A region as a modulating scaffold for p94/calpain 3 activity in skeletal muscle. *J. Biol. Chem. 283*, 14801–14814.
20. Richard, I., Broux, O., Allamand, V., Fougerousse, F., Chiannilkulchai, N., Bourg, N., Brenguier, L., Devaud, C., Pasturaud, P., Roudaut, C., et al. (1995) Mutations in the proteolytic enzyme calpain 3 cause limb-girdle muscular dystrophy type 2A. *Cell 81*, 27–40.
21. Beckmann, J. S., and Spencer, M. (2008) Calpain 3, the "gatekeeper" of proper sarcomere assembly, turnover and maintenance. *Neuromuscul. Disord. 12*, 913–921.
22. Sorimachi, H., Toyama-Sorimachi, N., Saido, T. C., Kawasaki, H., Sugita, H., Miyasaka, M., Arahata, K., Ishiura, S., and Suzuki, K. (1993) Muscle-specific calpain, p94, is degraded by autolysis immediately after translation, resulting in disappearance from muscle. *J. Biol. Chem. 268*, 10593–10605.
23. Rey, M. A., and Davies, P. L. (2002) The protease core of the muscle-specific calpain, p94, undergoes Ca^{2+}-dependent intramolecular autolysis. *FEBS Lett. 532*, 401–406.
24. Ma, H., Fukiage, C., Azuma, M., and Shearer, T. R. (1998) Cloning and expression of mRNA for calpain Lp82 from rat lens: splice variant of p94. *Invest. Ophthalmol. Visual Sci. 39*, 454–461.
25. Fougerousse, F., Bullen, P., Herasse, M., Lindsay, S., Richard, I., Wilson, D., Suel, L., Durand, M., Robson, S., Abitbol, M., Beckmann, J. S., and Strachan, T. (2000) Human-mouse differences in the embryonic expression patterns of developmental control genes and disease genes. *Hum. Mol. Genet. 9*, 165–173.
26. Fougerousse, F., Durand, M., Suel, L., Pourquié, O., Delezoide, A. L., Romero, N. B., Abitbol, M., and Beckmann, J. S. (1998) Expression of genes (CAPN3, SGCA, SGCB, and TTN) involved in progressive muscular dystrophies during early human development. *Genomics 48*, 145–156.
27. Herasse, M., Ono, Y., Fougerousse, F., Kimura, E., Stockholm, D., Beley, C., Montarras, D., Pinset, C., Sorimachi, H., Suzuki, K., Beckmann, J. S., and Richard, I. (1999) Expression and functional characteristics of calpain 3 isoforms generated through tissue-specific transcriptional and posttranscriptional events. *Mol. Cell. Biol. 19*, 4047–4055.
28. Ravulapalli, R., Campbell, R. L., Gauthier, S. Y., DhePaganon, S., and Davies, P. L. (2009) Distinguishing between calpain heterodimerization and homodimerization. *FEBS J. 276*, 973–982.
29. Ravulapalli, R., Diaz, B. G., Campbell, R. L., and Davies, P. L. (2005) Homodimerization of calpain 3 penta-EF-hand domain. *Biochem. J. 388*, 585–591.
30. Hosfield, C. M., Elce, J. S., Davies, P. L., and Jia, Z. (1999) Crystal structure of calpain reveals the structural basis for $Ca^{(2+)}$-dependent protease activity and a novel mode of enzyme activation. *EMBO J. 18*, 6880–6889.
31. Strobl, S., Fernandez-Catalan, C., Braun, M., Huber, R., Masumoto, H., Nakagawa, K., Irie, A., Sorimachi, H., Bourenkow, G., Bartunik, H., Suzuki, K., and Bode, W. (2000) The crystal structure of calcium-free human m-calpain suggests an electrostatic switch mechanism for activation by calcium. *Proc. Natl. Acad. Sci. U.S.A. 97*, 588–592.
32. Jia, Z., Petrounevitch, V., Wong, A., Moldoveanu, T., Davies, P. L., Elce, J. S., and Beckmann, J. S. (2001) Mutations in calpain 3 associated with limb girdle muscular dystrophy: analysis by molecular modeling and by mutation in m-calpain. *Biophys. J. 80*, 2590–2596.
33. Moldoveanu, T., Hosfield, C. M., Lim, D., Elce, J. S., Jia, Z., and Davies, P. L. (2002) A Ca^{2+} switch aligns the active site of calpain. *Cell 108*, 649–660.
34. Moldoveanu, T., Gehring, K., and Green, D. R. (2008) Concerted multi-pronged attack by calpastatin to occlude the catalytic cleft of heterodimeric calpains. *Nature 456*, 404–408.
35. Hanna, R. A., Campbell, R. L., and Davies, P. L. (2008) Calcium-bound structure of calpain and its mechanism of inhibition by calpastatin. *Nature 456*, 409–412.
36. DeLano, W. L. (2002)The PyMOL Molecular Graphics System, DeLano Scientific, San Carlos, CA (http://www.pymol.org).
37. Marti-Renom, M. A., Stuart, A., Fiser, A., Sánchez, R., Melo, F., and Sali, A. (2000) Comparative protein structure modeling of genes and genomes. *Annu. Rev. Biophys. Biomol. Struct. 29*, 291–325.
38. Van Der Spoel, D., Lindahl, E., Hess, B., Groenhof, G., Mark, A. E., and Berendsen, H. J. (2005) GROMACS: fast, flexible, and free. *J. Comput. Chem. 26*, 1701–1718.
39. Elce, J. S., Hegadorn, C., Gauthier, S., Vince, J. W., and Davies, P. L. (1995) Recombinant calpain II: improved expression systems and production of a C105A active-site mutant for crystallography. *Protein Eng. 8*, 843–848.
40. Cuerrier, D., Moldoveanu, T., and Davies, P. L. (2005) Determination of peptide substrate specificity for mu-calpain by a peptide library-based approach: the importance of primed side interactions. *J. Biol. Chem. 280*, 40632–40641.
41. Branca, D., Gugliucci, A., Bano, D., Brini, M., and Carafoli, E. (1999) Expression, partial purification and functional properties of the muscle-specific calpain isoform p94. *Eur. J. Biochem. 265*, 839–846.
42. Laskowski, R. A., Rullmannn, J. A., MacArthur, M. W., Kaptein, R., and Thornton, J. M. (1996) AQUA and PROCHECK-NMR: programs for checking the quality of protein structures solved by NMR. *J. Biomol. NMR 8*, 477–486.
43. Sorimachi, H., Kinbara, K., Kimura, S., Takahashi, M., Ishiura, S., Sasagawa, N., Sorimachi, N., Shimada, H., Tagawa, K., Maruyama, K., et al. (1995) Muscle-specific calpain, p94, responsible for limb girdle muscular dystrophy type 2A, associates with connectin through IS2, a p94-specific sequence. *J. Biol. Chem. 270*, 31158–31162.
44. Kinbara, K., Sorimachi, H., Ishiura, S., and Suzuki, K. (1997) Muscle-specific calpain, p94, interacts with the extreme C-terminal region of connectin, a unique region flanked by two immunoglobulin C2 motifs. *Arch. Biochem. Biophys. 342*, 99–107.
45. Murphy, R. M., and Lamb, G. D. (2009) Endogenous calpain-3 activation is primarily governed by small increases in resting cytoplasmic [Ca^{2+}] and is not dependent on stretch. *J. Biol. Chem.* (Epub ahead of print).

BI900130U